Journal of Drug Delivery Science and Technology 106 (2025) 106712

Contents lists available at ScienceDirect

Journal of Drug Delivery Science and Technology

journal homepage: www.elsevier.com/locate/jddst

# Bovine serum albumin (BSA)-Loaded polyvinyl alcohol (PVA) / chitosan (CH) / hydroxyapatite (HA) electrospun nanofibers for bone tissue regeneration

Mehmet Bozdag [a,b], Ferhat Urek [a,c], Sumeyye Cesur [a,b,*], Ali Sahin [d], Oguzhan Gunduz [a,b]

[a] Center for Nanotechnology & Biomaterials Application and Research (NBUAM), Marmara University, Turkey
[b] Department of Metallurgical and Materials Engineering, Faculty of Technology, Marmara University, Turkey
[c] Department of Bioengineering, Faculty of Life and Natural Sciences, Abdullah Gul University, Turkey
[d] Department of Biochemistry, School of Medicine/Genetic and Metabolic Diseases Research and Investigation Center, Marmara University, Istanbul, Turkey

ARTICLE INFO

*Keywords:*
Nanofibers
BSA
HA
Osteoblast regeneration
Bone tissue regeneration

ABSTRACT

The natural bone structure consists of three different nanocomposite layers; a porous polymer ceramic part, a lamellar, and a fiber-matrix composition gives the bone its unique physical and biological properties. During bone tissue regeneration bioactivity, and osteoinductivity are especially important with other parameters such as porosity, degradation rate, and cell adhesion. In this study, hydroxyapatite (HA) and bovine serum albumin (BSA) protein-loaded, polyvinyl alcohol (PVA) and chitosan (CH) nanofibers were fabricated via the electrospinning method. The mean diameters of PVA/CH/HA/BSA-5, PVA/CH/HA/BSA-10, and PVA/CH/HA/BSA-15 nanofibers were measured as 325.39 ± 77.512 nm, 332.45 ± 82.251 nm, 447.03 ± 101.382 nm respectively, required porosity and properties for bone tissue engineering were considered achieved. BSA release profiles of BSA-5, BSA-10, and BSA-15 nanofibers were similar in terms of burst release which continued until the 12th hour, 58 %, 78 %, and 73 % of the BSA were released, respectively. After 72 h 100 % of BSA were released from all nanofibers. Cell viability tests showed that PVA/CH/HA/BSA nanofibers exceeded the control group in terms of cell viability by 119.9 %. In future bone injury treatment, PVA/CH/HA/BSA nanofibers can assist the healing process of cracks and fractures, and decrease the recovery time of bone as an alternative bone healing nanofiber.

## 1. Introduction

The natural bone structure is hard to mimic because of its complex structure, a combination of inorganic materials, organic materials, and fibrous-shaped extracellular materials; such as collagen and hydroxyapatite. Porosity, resorbability, degradation and cell adhesion properties of the scaffold must be considered additional to osteoconductive and osteoinductivity in order to fabricate a desirable scaffold with suitable mechanical and degradation properties for bone tissue [1,2]. The traditional autologous and heterologous grafts as bone replacements still have limitations such as availability, compatibility, and immune reactions [3,4]. Usage and fabrication of organic-inorganic biomaterials, tissue-engineered 3D structures with proper availability, biomimicry, and low immunogenicity can overcome traditional limitations of metallic and/or surgical methods.

The electrospinning method, via nano to micro-scale fiber fabrications with desired mechanical strength and properties, gives a huge advantage to mimic the bone tissue. And to create a scaffold for cell regeneration and adhesion [3,5,6]. The electrospinning technique allows the fabrication of nano to micro-scale fibrous structures with slight diameters by using a polymeric fluid pumped to a collector, under electrical field presence. The polymeric solution solidifies and creates fibers due to the interactions of the electrical field applied. By using the electrospinning method, it is possible to create desired mono and multi-layer scaffolds with various polymer combinations with bioactive materials to promote bone tissue regeneration [7].

In order to mimic the natural bone ECM, bioactive and polymeric biomaterials of the scaffold must be chosen carefully. The inorganic part of the bone ECM, the hard tissue, is made from hydroxyapatite (HA, $Ca_5(PO_4)_3OH$), which is both biocompatible, inflammatory, and osteoconductive [8]. Since it is a constituent of bone, HA is widely used for metallic implant coatings, bone fillings, injectable bone biomaterials,

* Corresponding author. Center for Nanotechnology & Biomaterials Application and Research (NBUAM), Marmara University, Turkey.
*E-mail address:* sumeyye.cesur@marmara.edu.tr (S. Cesur).

https://doi.org/10.1016/j.jddst.2025.106712
Received 18 July 2024; Received in revised form 30 December 2024; Accepted 12 February 2025
Available online 14 February 2025

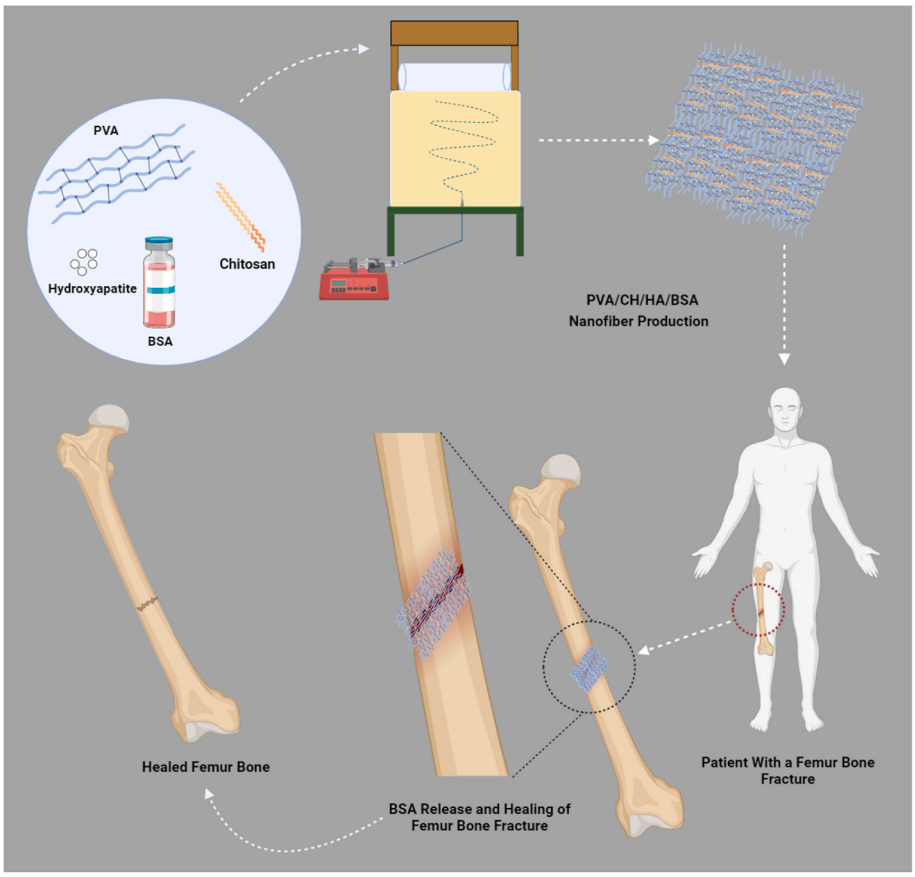


**Fig. 1.** Schematic illustration of PVA/CH/HA/BSA nanofibers fabrication process via electrospinning for bone tissue.

and as bioactive particles in scaffolds. HA usage in many different 3D structures in order to initiate and/or increase bone tissue regeneration is well known [5,9]. Bal et al. [9], explain that HA nanocrystals increase the surface area for cells to attach and grow, and increase the cell-to-cell connection, migration, signaling, and differentiation. And Rajzer et al. [10], mention the PLDL fibers loaded with HA nanoparticles and prove the addition of HAp increases cell attachment, cell proliferation, and osteoblastic differentiation.

To maintain good mechanical properties and increase biocompatibility, different organic polymers with varying attributes are widely used in fiber fabrication during electrospinning. Polyvinyl alcohol (PVA) is a polymer regularly used in tissue engineering for nanofiber fabrication, dressing, and 3D structure production due to its biocompatibility, hydrophilicity, biodegradation, and good mechanical properties [11]. Asran et al. [12], present a PVA/Collagen and HA nanofiber scaffold fabricated for natural bone, proving that PVA and HA are compatible to form HA crystals along the fibers and mimics the structure of bone ECM. In another study, Kim et al. [13], introduce PVA/HA and mention the crystalline structures formed by HA along PVA fibers increase the thermal stability and act as building blocks for bone tissue. For the fabrication of fibers, PVA was selected as a main polymer due to its crystalline forming ability with HA to increase cell adhesion and proliferation, with other properties such as; biocompatibility, biodegradability, mechanical and water uptake, and good fiber-forming properties.

Chitosan (CH) is another polymer drawn a lot of attention due to its biocompatibility, biodegradability, gelation, adhesion, and non-toxic properties. In the last decades, CH has been widely used for many medical applications including bone and skin tissue applications, wound healing, and dressings [14]. Shirzaei et al. [15], present CH/PCL/HA electrospun fibers for bone tissue, proving that CH exhibits good effects on cell adhesion and pore size, and corporates with HA addition to increase the bioactivity and degradability. Due to unique bio adhesion and biomineralization properties among its biocompatibility, biodegradation, and gelation properties; chitosan was selected as the secondary polymer in low concentrations for nanofiber fabrication.

Bovine serum albumin (BSA) is a protein used nowadays, in applications such as tissue engineering, wound healing, drug delivery, and biosensor applications. In blend mixing of such proteins is expected to enhance the tissue applications performance and pore formations on fibers for enhanced cell attachment and connection [16,17]. With the dissolution of BSA from the nanofiber, generated biochemical signals can expected to mimic ECM to enhance cell proliferation [18].

In this study, PVA/CH/HA/BSA blend nanofibers with various BSA concentrations (0.05, 0.1, and 0.15 wt%) were fabricated via electrospinning method to treat bone cracks/fractures and to enhance bone tissue regeneration, as illustrated in Fig. 1. The PVA/CH/HA/BSA nanofiber scaffold structures were designed to be used as scaffolds to trigger the bone healing process, and provide both mechanical and biological support to the damaged bone tissue. Such nanofiber structures can be stacked and layered for scaffold designing or could used in form of mashes of fibers in order to fill the cavities/gaps formed due to infections, wounds, and etc. on the bone tissue. The primary objective of the present study is to observe the effects of protein bovine serum albumin (BSA) with various concentrations on bone tissue regeneration and the use of BSA with hydroxyapatite (HA) biomineral within biodegradable, porous, nanofibre mat-like scaffold structures. The addition of BSA and HA was intended to increase the overall cellular regeneration and attachment performance. It is hypothesised that HA will cause biomineralization and result in porous structures. BSA was included to stimulate cellular interactions for enhanced osteogenesis and to provide the necessary osteogenic cells to the site of defection. Moreover, we

**Table 1**
Contents of all nanofibers produced.

| Nanofibers | PVA Content [wt.%] | CH Content [wt.%] | HA Content [wt.%] | BSA Content [wt.%] |
|---|---|---|---|---|
| PVA/CH | 13 | 1 | 0.05 | 0 |
| PVA/CH/HA | 13 | 1 | 0.05 | 0 |
| PVA/CH/HA/BSA-5 | 13 | 1 | 0.05 | 0.05 |
| PVA/CH/HA/BSA-10 | 13 | 1 | 0.05 | 0.1 |
| PVA/CH/HA/BSA-15 | 13 | 1 | 0.05 | 0.15 |

**Table 2**
Electrospinning parameters of each nanofiber fabricated.

| Nanofibers | Voltage (kW) | Flow Rate (ml/h) |
|---|---|---|
| PVA/CH | 26.5 | 0.2 |
| PVA/CH/HA | 29 | 0.3 |
| PVA/CH/HA/BSA-5 | 29 | 0.38 |
| PVA/CH/HA/BSA-10 | 26 | 0.3 |
| PVA/CH/HA/BSA-15 | 27 | 0.3 |

propose that the release of BSA from PVA/CH/HA/BSA-composed nanofibers will enhance osteoblast cell proliferation increase the porosity of fiber with time, and assist healing of the injured bone tissue.

## 2. Materials and methods

### 2.1. Chemicals

Polyvinyl alcohol (PVA, Mw: 89–98 kDa, 99 % hydrolyzed), chitosan (CH), hydroxyapatite (HA, Mw: 502,31 g/mol), phosphate-buffered saline (PBS, pH = 7.4), glutaraldehyde solution (GA, 50 wt% Mw = 100.12 g/mol), and acetic acid were produced by Sigma-Aldrich (St. Louis, MO, USA). Bovine serum albumin (BSA) was purchased from AFG Bioscience LLC (Northbrook, IL, USA).

### 2.2. Solution preparation for electrospinning

A variety of solutions with different concentrations of BSA were arranged according to the specifications in Table 1. A 13 wt% PVA solution was prepared using distilled water in conjunction via a magnetic mixer (Wise Stir, MSH-20, Germany) operating at 240 revolutions per minute (rpm) and 150 °C (°C) for 2 h. Additionally, a 1 wt% CH solution was prepared by mixing Acetic acid and distilled water at a 1:100 ratio, followed by stirring via a magnetic mixer at 240 rpm and 50 °C, 2 h long. Subsequently, the PVA and CH solutions were blended in a 9:1 vol ratio and stirred for 45 min at 240 rpm and 40 °C. Afterward, 0.5 wt% HA powder was introduced into the PVA/CH solution and stirred for an additional 30 min at 200 rpm and 35 °C. Following this, BSA solutions with concentrations of 0.05, 0.1, and 0.15 wt% were prepared and stirred for 30 min at 200 rpm and 35 °C.

### 2.3. Nanofiber fabrication and Cosslinking

In the nanofiber fabrication process, we utilized a lab-scale electrospinning apparatus (NS24, Invens Co., Turkey). Each blend solution underwent optimization procedures during electrospinning. The solution was loaded into a syringe which was then connected to a pump, with the flow rate set at 0.3 mL per hour (ml/h). A rotating cylindrical collector positioned 12 cm away from the metallic surface holding the needles, was employed to gather the nanofibers. Before the electrospinning process, the collector was enveloped with wax paper, and its weight was recorded. Electrospinning experiments were conducted using different combinations of flow rates and voltages, as delineated in Table 2. The crosslinking process of the nanofibres was conducted using 25 % GA vapor. The nanofibres were meticulously positioned within a desiccator above the GA solution and subjected to incubation for a period of 5 h at 40 °C (°C) in an oven. Subsequent to the production stage, the fibres were washed thrice with Phosphate Buffered Saline (PBS). The washing process was carried out by immersing the fibres in PBS and removing them in order to avoid any adverse effects on the drug release. This method was employed to attempt to remove glutaraldehyde from the fibres. It can be concluded that the washing process had no toxic effect on the cells and that the glutaraldehyde was successfully removed.

### 2.4. Scanning electron microscopy (SEM)

The surface morphologies of the fabricated nanofibers were examined by scanning electron microscopy (SEM, EVO LS 10, Zeiss). First, a layer of gold and palladium was applied to the surface of each nanofiber for 2 min using a spray coating apparatus (Quorum SC7620, USA). Subsequently, histogram graphs were generated based on the 100 fibers measured in SEM results by using imaging software (Olympus AnalySIS, USA).

### 2.5. Fourier transform infrared spectroscopy (FT-IR)

A Fourier-transformed infrared spectroscopy (FTIR) (FT/IR-4700, Jasco) was utilized to examine the chemical properties of the nanofibers. The spectra were logged and carried out at room temperature(23 °C). The transmission procedure was set to be at scanning speed 32, and scanning resolution was set as 4 $cm^{-1}$, and the scanning was performed at 4000–400 $cm^{-1}$ intervals.

### 2.6. Differential Scanning Calorimetry (DSC)

To scrutinize the glass transition temperature (Tg) and melting temperature (Tm) of the nanofibers, Differential Scanning Calorimetry (DSC) (Shimadzu, Japan) was employed. The altering response of the material to thermal stimuli was evaluated by subjecting nanofibrous samples to the DSC apparatus, encompassing a temperature range from 25 to 300 °C (°C) and 100 different heating rates.

### 2.7. Mechanical analysis of nanofibers

For the assessment of the mechanical characteristics of individual nanofibers, a tensile testing apparatus (Shimadzu Corporation, EZ-LX, Kyoto, Japan) was employed. Before conducting the tensile test, the thickness of the nanofibrous patches was determined utilizing a digital micrometer (Mitutoyo MTI Corp., USA). Subsequently, the samples were resized to dimensions of 10 × 50 mm (mm). Each group underwent testing with three distinct samples to ensure reliability and consistency in the results.

### 2.8. Swelling and degradation behavior of PVA/CH/HA/BSA nanofibers

To evaluate the water-absorbing capability of the fabricated nanofibers and monitor alterations in their mass over time in solution, swelling and degradation assessments were conducted. Phosphate-buffered saline (PBS) with a pH of 7.4 served as the swelling test solution. Nanofibers of equal weight were put inside 1 ml of PBS, into Eppendorf tubes, further maintained at 37 °C (°C) within a thermal shaker (TS-100, BIOSAN). Subsequent to a day (24h) incubation period, the nanofibers were extracted from the excess PBS, and damp amounts were recorded. Equation (1) was employed for the computation of the water intake extent [19].:

$$S = \frac{Ww - Wo}{Wo}.100 \quad \text{eq (1)}$$

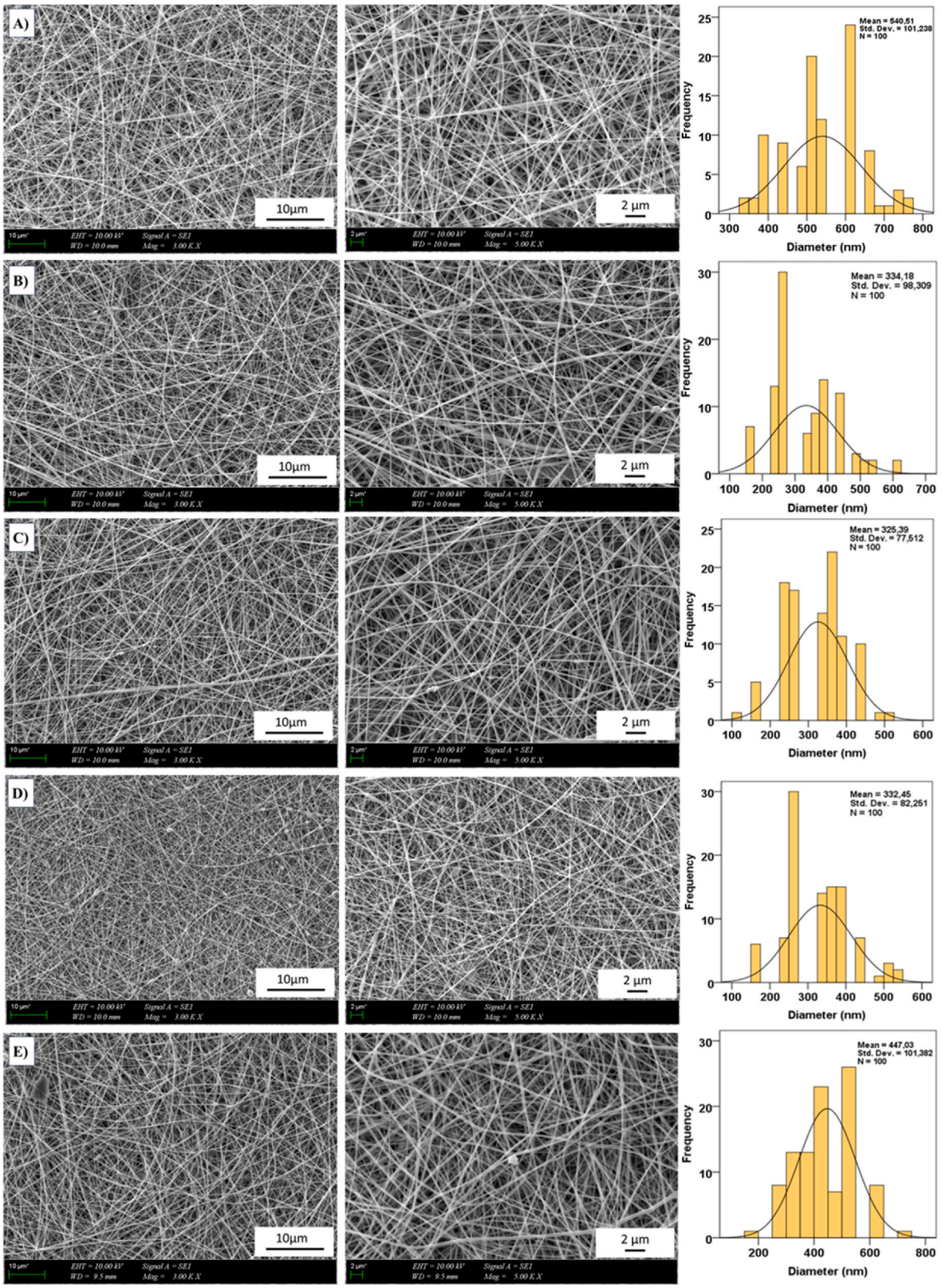


**Fig. 2.** Morphological images of nanofibrous patches obtained by SEM and histogram graphs of diameters; PVA/CH (A), PVA/CH/HA (B), PVA/CH/HA/BSA-5 (C), PVA/CH/HA/BSA-10 (D), PVA/CH/HA/BSA-15 (E).

For the degradation investigation, nanofibrous patches of uniform weight were selected and immersed in PBS within 1 ml Eppendorf tubes, utilizing a thermal shaker device. Following a 24-h period, the PBS was decanted from the samples, and the nanofibers were subjected to drying in a thermal shaker for an additional 24 h. Subsequently, the degradation of the nanofibers was calculated based on the equation, considering the weights measured post-drying ($W_t$) (2) [20]:

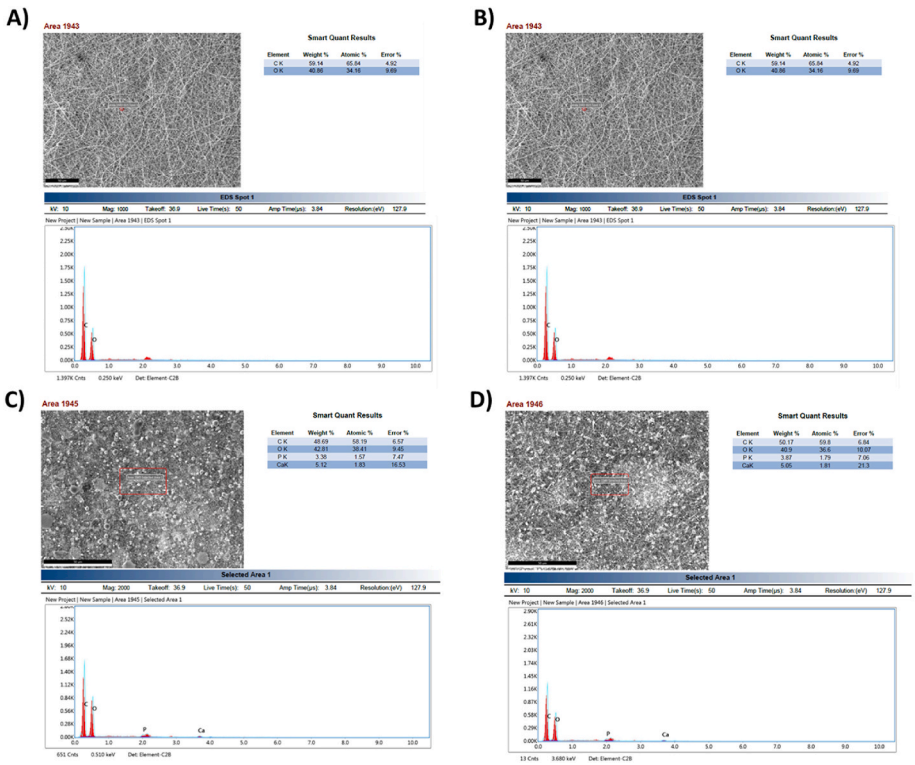


**Fig. 3.** SEM/EDX results showing HA presence in applied samples, obtained from A) PVA/CH, B) PVA/CH/HA/BSA5, C) PVA/CH/HA/BSA10, D) PVA/CH/HA/BSA15 samples.

$$D = \frac{Wo - Wt}{Wo}.100 \quad \text{eq (2)}$$

### 2.9. Cell culture test

#### 2.9.1. Sterilization of materials

Material sterilization was conducted using UV light for a duration of 90 min within a class II laminar flow cabinet. Following the UV sterilization period, the materials were transferred to a 96-well plate containing a 20 μl medium to verify their stability.

#### 2.9.2. Cell culture test

The electrospun nanofibers underwent UV light exposure overnight to ensure sterilization before being transferred into 96-well plates. Following this, they were immersed in a cell culture medium and allowed to incubate for a period of 2 h to promote cellular adherence. Human osteoblast cells (ATCC hFOB 1.19 CRL-3602 ™) were then seeded onto the nanofibers and maintained at a temperature of 37 °C with 5 % $CO_2$ to facilitate cell adhesion and viability assessment. The MTT test, a standard method for evaluating cell viability, was conducted at intervals of 1, 4, and 7 days post-incubation, following the manufacturer's methodology. The absorbance readings at 570 nm were obtained using an ELISA reader (Enspire, PerkinElmer) to quantify cytotoxicity levels. Each assay was repeated thrice, and the mean values were calculated. Prior to the MTT assay, the nanofibers were rinsed with PBS solution (pH 7.4), and then treated with 0.5 ml (0.5 mg/ml) of MTT solution, followed by incubation for 5 h at 37 °C with 5 % $CO_2$. Subsequently, the supernatant was carefully removed, and 1.5 ml of dimethyl sulfoxide (DMSO) was added. The plates were incubated again for 15 min at 37 °C under 5 % $CO_2$ conditions, and absorbance measurements at the wavelength 560 nm were recorded via a microplate reader.

#### 2.9.3. Scanning electron microscopy imaging

Following the completion of the cell culture experiments, fixation of the cells on the nanofiber structure was achieved using a fixation solution composed of an acetic acid: methanol mixture in a 1:3 ratio. Then the medium solution was removed prior to the fixation operation, and the nanofibers were rinsed twice with PBS. Subsequently, the fixation solution was applied, and the nanofibers were incubated at room temperature on a shaker for 10 min. Upon completion of the incubation, the fixation mixture was discarded, and the nanofibers were rinsed twice with distilled water. Subsequent to this, the nanofibers were prepared for imaging utilizing an SEM (EVO LS 10, Zeiss) operated at 10 kV.

### 2.10. In vitro BSA release

To conduct in vitro BSA discharge evaluations, 5 mg of BSA-loaded nanofibers were introduced into 1 ml of PBS and maintained at 37 °C temperature within the thermal shaker (TS-100, BIOSAN, Riga, Latvia). UV spectrophotometer assessment were performed in predetermined time durations. To sustain the ongoing release studies, the PBS solution was replenished with fresh 1 ml PBS at each measurement point.

### 2.11. BSA release kinetics of nanofibers

The mathematical models used to evaluate drug release kinetics are zero order, first order, Korsmeyer-Peppas, Higuchi, and Hixson-Crowell equations [21];

$$Q = Kt^n \quad \text{eq (3)}$$

$$Q = K_0 t \quad \text{eq (4)}$$

$$\ln(1-Q) = -K_1 t \quad \text{eq (5)}$$

$$Q = K_h t^{1/2} \quad \text{eq (6)}$$

$$Q^{1/3} = K_{hc} t \quad \text{eq (7)}$$

In given equations, the dependent variable is the amount of drug released at time t, denoted with the letter "Q". The kinetic constants of the Zero-order, First-order, Korsmeyer-Peppas Higuchi, and Hixson-

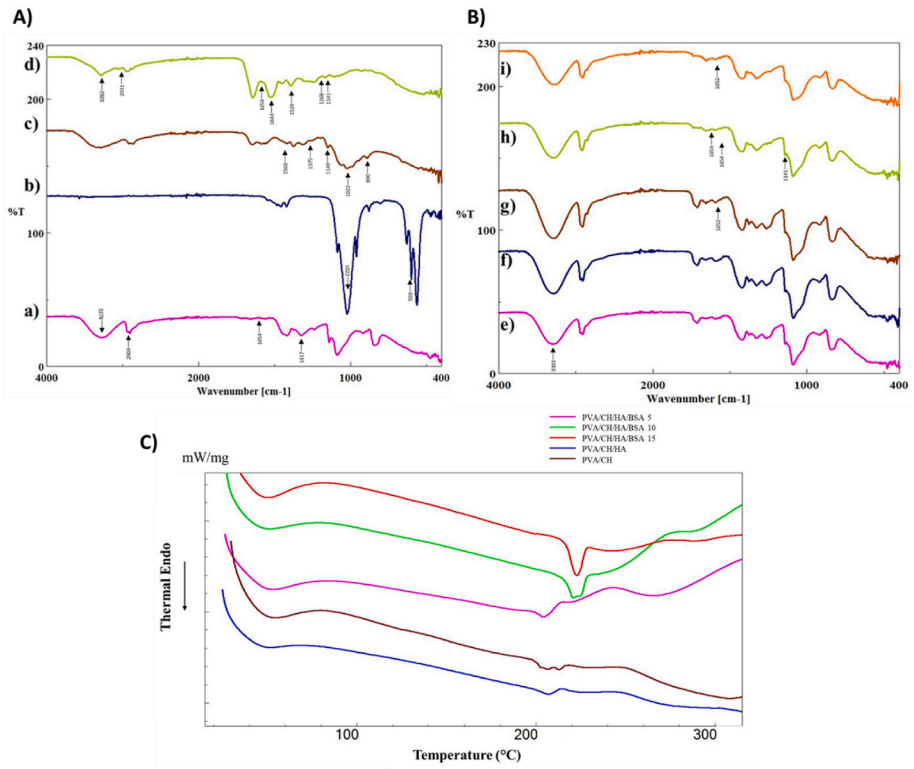


**Fig. 4.** FTIR spectra of pure PVA ((A)), a), pure CH ((A)), b), HA ((A)), c), BSA ((A)), b); FTIR spectra of nanofibers PVA/CH ((B)), e), PVA/CH/HA ((B), f), PVA/CH/HA/BSA-5 ((B), g), PVA/CH/HA/BSA-10 ((B), h), PVA/CH/HA/BSA-15 ((B), i) nanofibers; DSC thermograms of the nanofibers (C).

Crowell equations, represented by "$K_0$," "$K_1$," "$K_h$," and "$K_{hc}$," respectively, are used to calculate the aforementioned dependent variable. And the diffusion exponent, represented by "n", reveals the drug release system.

### 2.12. Statistical analysis

Statistical analysis was conducted using a single-factor ANOVA program, while pore size measurements were performed using SPSS 17.0 analysis software. A significance level of $p < 0.05$ was accepted for statistical inference, and the data were submitted in a manner that included both their respective means and standard deviations.

## 3. Results and discussion

### 3.1. Scanning electron microscope (SEM)

Surface morphologies of nanofibers were investigated using SEM analysis. For diameter measurements, 100 different fibers were chosen to measure from every sample, and the obtained measurements are presented in the histogram in Fig. 2. And The SEM results in Fig. 2, indicated that nanofibers with and without BSA and HA showed smooth surface and monodispersed fiber formation. Among the samples fabricated, PVA/CH/HA/BSA-5 fibers exhibited the thinnest fibers, while PVA/CH fibers were the thickest. The mean diameters of PVA/CH, PVA/CH/HA, PVA/CH/HA/BSA-5, PVA/CH/HA/BSA-10, PVA/CH/HA/BSA-15 nanofibers were measured as 540.51 ± 101.238 nm, 334.18 ± 98.309 nm, 325.39 ± 77.512 nm, 332.45 ± 82.251 nm, 447.03 ± 101.382 nm respectively. Results indicated that the fibers PVA/CH/HA, PVA/CH/HA/BSA-5, and PVA/CH/HA/BSA-10 showed a decrease in the diameters with the addition of a certain amount of HA and BSA when compared to the pure and highest BSA-loaded fiber samples. Satpathy et al. mentioned that loading HA to PVA/CH blend fibers can cause a change in the diameter. The PVA/CH fiber was 395 ± 162 nm, after the HA addition the fiber diameter decreased to 300 ± 121 nm [1]., Salim et al. mention the addition of HA to PVA/Hyaluronan fibers caused few bead formations and uniform fiber structures with less porous area [22]. Fazel et al. reported that PVA/BSA blend fibers can exhibit changes in fiber diameters ranging from 200 to 500 nm and cause bead formations with 7 m in length and ~1.5 m in diameter [23]. Another study by Zang et al. confirmed that the addition of aspirin or BSA can cause bead formations due to their effects on PVA [24]. In order to provide presence of HA in applied samples, SEM/EDX measurements performed. As illustrated in Fig. 3, the samples were subjected to SEM/EDX analysis. The samples lacking an HA context (PVA/CH) and the samples with an applied HA context (samples with both HA and BSA) are presented. The SEM/EDX results demonstrate that the PVA/CH samples do not contain HA, while the presence of HA is evident through the detection of P and Ca.

### 3.2. Fourier transform infrared spectroscopy (FT-IR)

The FTIR was used for molecular structural examination of PVA/CH, PVA/CH/HA, and all PVA/CH/HA/BSA nanofibers. In Fig. 4A(a), for pure PVA sharp peaks and strips were observed at 3278 cm-1 complying with the O-H bonding, at 2904 cm-1 C-H bond of alkyl groups, at 1654 cm-1 the acetate group, C-O and C=O bonds, and at 1417 cm-1 C-$H_2$ bond [21]. In Fig. 4A(b), for pure CH the sharp band at 1022 cm-1 indicates the CH saccharide structure, at 1149 and 890 cm-1 indicates C-N and C-H amide group, at 1560 cm-1 is related to N-H bending, and 1375 cm-1 is proof of OH ring of CH stretching [25]. In Fig. 4A(c), for pure HA the sharp peaks at 1022 cm-1 and 593 cm-1 indicate the phosphate stretching and bending [1]. In Fig. 4A(d), for the BSA multiple peaks at 3282 cm-1 and 2931 cm-1, amide A and amide B, indicate the N-H stretching. At 1644 cm-1 amide I, the C=O stretching, at 1529 cm-1 amide II, the C-N and N-H stretching and bending [26]. In Fig. 4B(e), the obtained PVA/CH spectrum shows a resemblance with pure PVA and CH spectrum, the peak present at 3278 cm-1 in pure PVA shifted to 3303

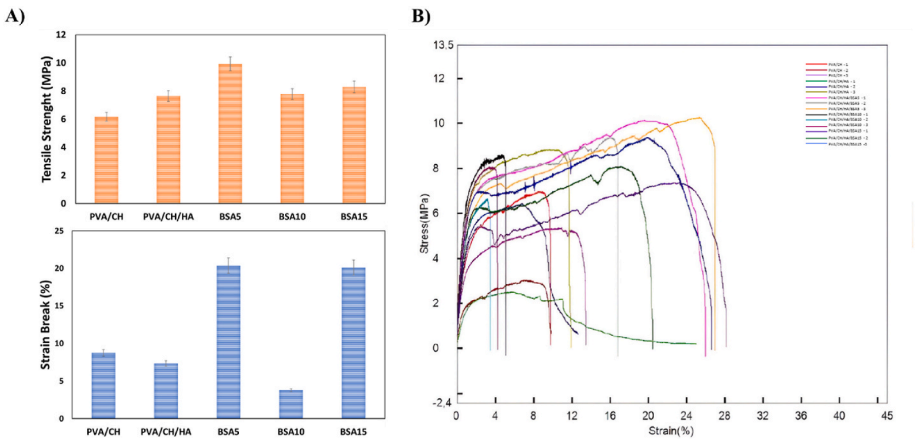


**Fig. 5.** Tensile test measurements of the nanofibers: (A) tensile strength and strain at break, (B) stress-strain curve.

cm-1 with CH addition [1]. Fig. 4B(f), the spectrum of the PVA/CH/HA sample, the inclusion of HA showed a minor impact in spectra, Fig. 4B (g), PVA/CH/HA/BSA-5 sample, the spectrum also has similarities with pure PVA, CH, and BSA spectrum, at 1652 cm-1 vibration caused by BSA addition can be seen. In Fig. 4B(h), the spectrum of PVA/CH/HA/BSA-10 also shows a resemblance with previous spectrums, the peak at 1654 cm-1 indicated the effect of BSA addition, and 1168 cm-1 at pure BSA spectrum is shifted to 1141 cm-1. And Fig. 4B(i), the spectrum of PVA/CH/HA/BSA-15 same peak from BSA-5 and BSA-10 samples present at 1652 cm-1. Thus, the nanofibers with BSA and HA were fabricated successfully.

### 3.3. *Thermal properties*

Thermal measurement techniques are crucial tools to understand and determine the physical and chemical changes of investigated material, changes such as phase transition, glass transition temperature (Tg), and melting temperature (Tm) [27]. DSC thermograms of each electrospun

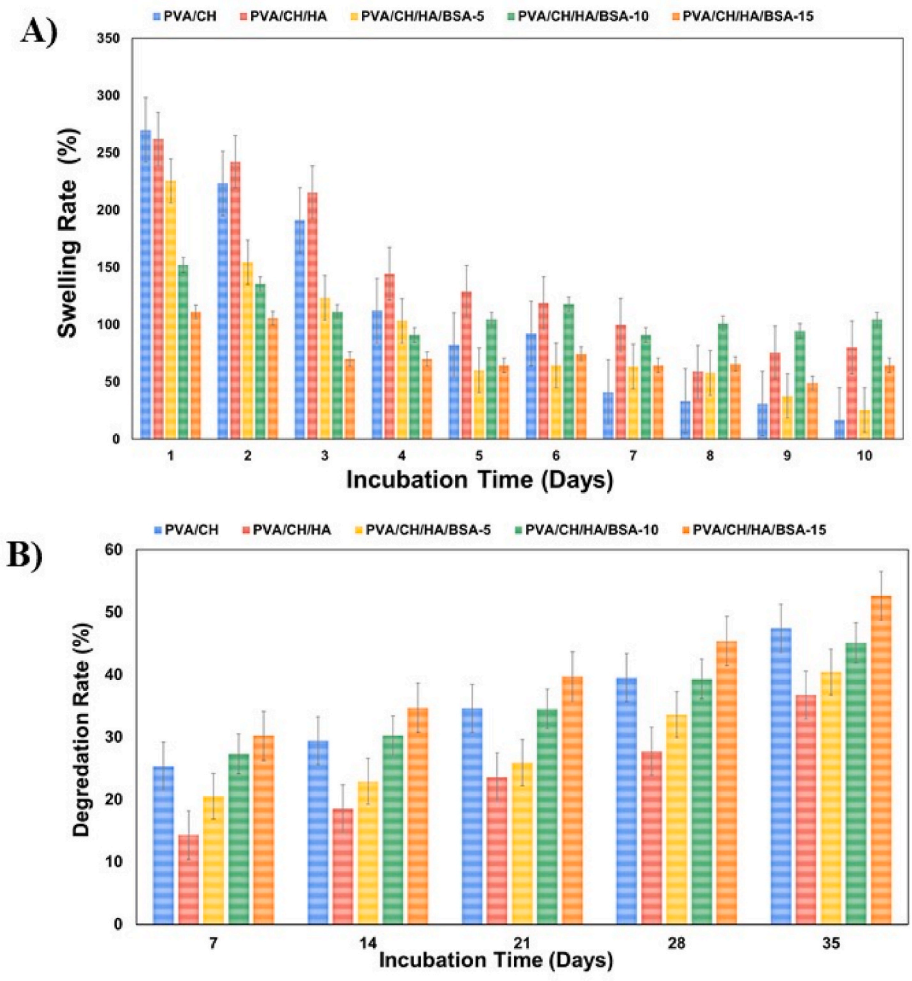


**Fig. 6.** Swelling (A) and degradation (B) behaviors of each nanofiber produced.

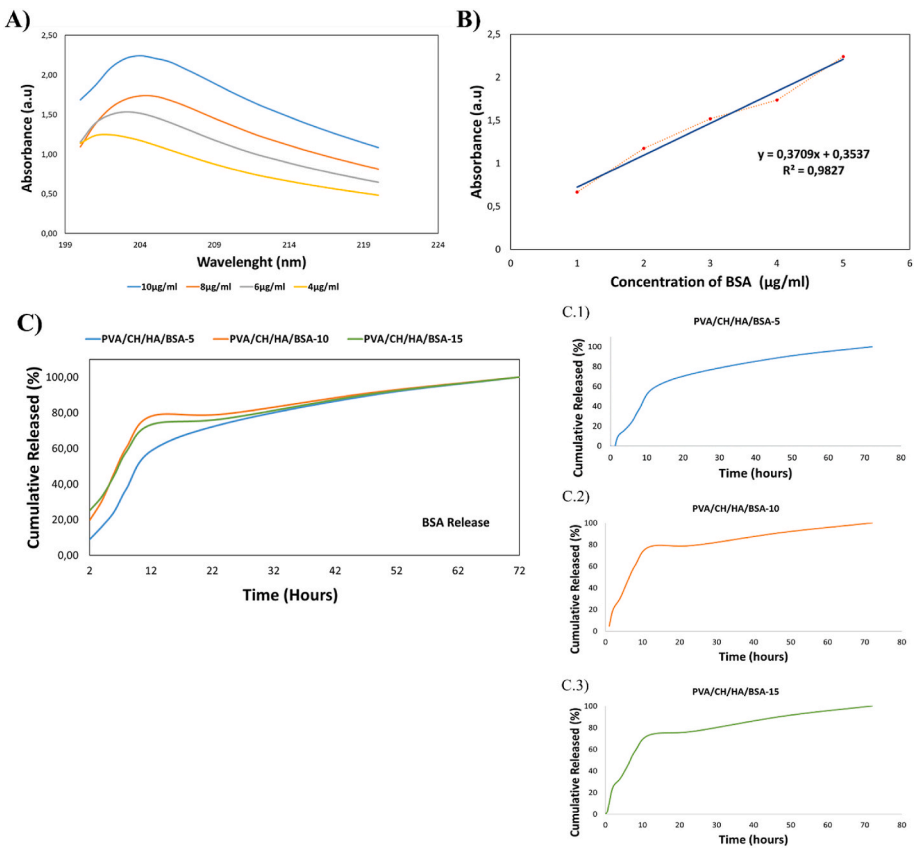


**Fig. 7.** In vitro BSA release profiles of PVA/CH/HA/BSA nanofibers: Absorption spectra of BSA at different concentrations (A), BSA calibration curve (B), BSA release profiles from the PVA/CH/HA/BSA electrospun nanofibers (C); BSA-5 (c.1.), BSA-10 (c.2.), and BSA-15 (c.3.) samples shown detailed. All measurements were repeated three times.

nanofiber, PVA/CH, PVA/CH/HA, PVA/CH/HA/BSA-5, PVA/CH/-HA/BSA-10, and PVA/CH/HA/BSA-15 are shown in Fig. 4 (C). PVA (polyvinyl alcohol) represents a polymer with a partially crystalline structure, which can be observed to exhibit both a glass transition temperature, $T_g$, and a melting isotherm, $T_m$ [21]. The peaks observed during the DCS analysis were mainly caused by PVA, which is the main ingredient with the highest concentration in all nanofibers fabricated. The peak observed at 210 °C in the thermogram for the PVA/CH and PVA/CH/HA nanofibers correlates with the melting temperature for PVA. And the small curved peaks occurred until 80 °C due to glass transitioning of PVA which happens between 49 and 63 °C but including the CH within the context may shift the peak along the right side [21, 28]. Koosha and Mirzadeh, mention similar changes during the thermal analysis of CH/PVA electrospun due to water molecules present in CH which can liberate in various temperatures [28]. Glass transition temperatures for PVA/CH/HA/BSA-5, PVA/CH/HA/BSA-10, and PVA/CH/HA/BSA-15 nanofibers were 75.30, 67.18, and 73.43, respectively. And melting point temperatures for PVA/CH/HA/BSA-5, PVA/CH/HA/BSA-10, and PVA/CH/HA/BSA-15 nanofibers were measured as 205.45, 220, 223.63, respectively. Risdian et al. mention, that after BSA addition Tg and Tm values change slightly due to the hydrogen bond between PVA chains and BSA molecules, which causes to Tm value to get slightly higher and changes in Tg value [26].

### 3.4. Mechanical properties

The mechanical properties of the PVA/CH, PVA/CH/HA, and all PVA/CH/HA/BSA were investigated to understand the durability and resistance of fabricated nanofibers. Each nanofiber sample was measured and analyzed in terms of both tensile strength and elongation at break, results shown in Fig. 5. The PVA/CH nanofibers showed a tensile strength of 6.16 ± 0.81 MPa and a strain break value found 8.72 ± 1.4. When HA was introduced to the nanofiber content, PVA/CH/HA had a tensile strength of 7.65 ± 1.21 MPa, and a strain break value of 7.34 ± 1.69 was found. For PVA/CH/HA/BSA-5, PVA/CH/HA/BSA-10, and PVA/CH/HA/BSA-15 nanofibers the tensile strengths were 9.93 ± 0.40, 7.78 ± 0.82, and 8.28 ± 0.83, respectively. And the strain breaks for each BSA-loaded sample, were 20.36 ± 3.83, 3.77 ± 0.65, and 20.09 ± 2.45, respectively. It is possible to say the addition of HA into PVA/CH nanofiber increased its tensile strength. Salim et al. mentions similar observations after the addition of HA to PVA/Hyaluronic Acid electrospun nanofibers they produced, the tensile strength increased [22]. With the addition of BSA to the PVA/CH/HA blend, the mechanical properties slightly increased for BSA-5 and decreased for both BSA-10&15 samples. The addition of BSA, even in small amounts, can cause a decrease in mechanical properties. Li et al. mention the addition of BSA-dextran to PLGA nanofibers and indicate similar results, a decrease in mechanical properties [29]. Another work by Bercea et al. mentions addition of BSA to a polymeric blend can cause a reduction of the viscoelastic modulus and shear viscosity [30].

### 3.5. Swelling and degradation behavior

Absorption capabilities of the nanofibers were tested in order to understand the capacity for transportation of molecules such as; oxygen and other molecules. Fig. 6A reports the PBS uptake amounts of each nanofiber at 37 °C for 10 days. In Fig. 6A, it can be seen that PVA/CH nanofiber exhibits a decreasing water-uptake profile up to the 5th day and then starts to degrade. PVA/CH/HA fiber also exhibits similar behavior to PVA/CH nanofibers, with swelling behavior up to the 7th day. PVA/CH/HA/BSA-5 nanofiber exhibits similar behavior to PVA/CH and PVA/CH/HA and presents a similar decreasing swelling rate until

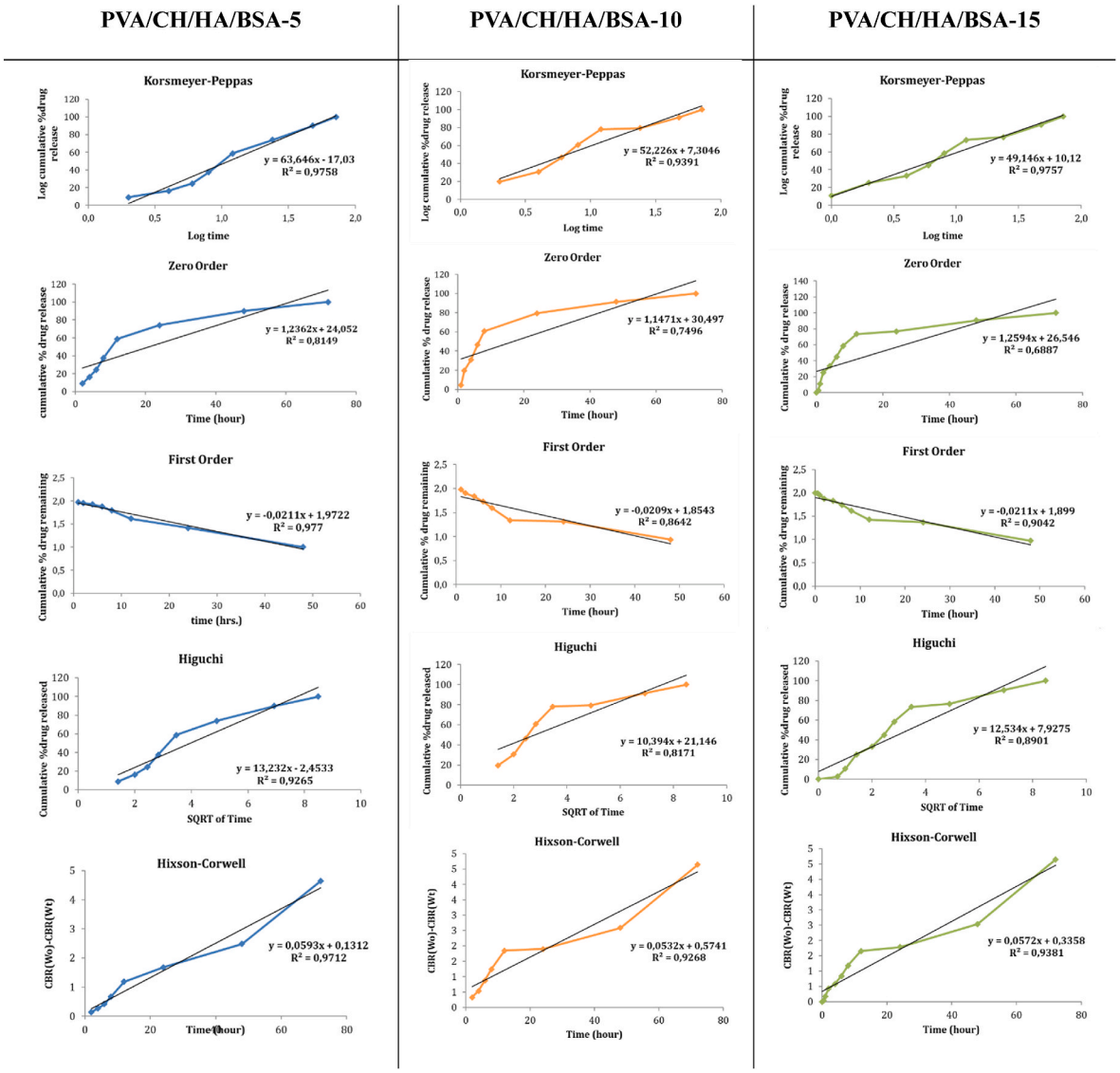


**Fig. 8.** In vitro release kinetic models of the PVA/CH/HA/BSA-5, PVA/CH/HA/BSA-10, and PVA/CH/HA/BSA-15 scaffolds.

the 8th day with the highest swelling rate at 220 % on the 1st day. PVA/CH/HA/BSA-10 and PVA/CH/HA/BSA-15 samples showed different swelling behaviors than other samples, continuing their swelling behavior until the 10th day. For PVA/CH/HA/BSA-10 nanofiber, reached a swelling rate of 150 % on the 1st day and slowly decreased and stabilized on the 4th day at around 100 % swelling rate until the 10th day. Similarly, PVA/CH/HA/BSA-15 nanofiber exhibits relatively stable swelling behavior, reaching a maximum swelling rate of 100 % on the 1st and 2nd day, and stabilizing around 70 % until the 10th day. Overall, among all nanofibers, PVA/CH showed the highest swelling rates of 250 % for the initial day, this might happen because of CH content, which can decrease the crystallization degree of PVA [31]. Among PVA/CH/HA/BSA nanofibers, BSA-10 showed a 100 % swelling rate for the 4th to 10th day.

Degradation is an essential process for tissue engineering applications due to the need for the disappearance of the scaffold after the necessary cultivation of cells occurs successfully [21]. The degradation properties of each nanofiber fabricated were investigated and shown in Fig. 6B. According to Fig. 6B, as a result of the degradation of nanofiber groups, the pure group consisting of PVA/CH showed a degradation rate of 47.4 % at the end of 35 days, while the rate decreased by 36.7 % with the inclusion of HA in the structure. It was observed that HA slowed down the degradation process by increasing the integrity of the matrix. Ma et al. performed an analysis with Gel/CS/PVA composite scaffold and hydroxyapatite, the results obtained from physical characterization on four samples with various HA amounts show similar results to those obtained in our study, the degradation process slows down as the HA content increases [32]. In addition, when the PVA/CH/HA/BSA groups are examined, the water permeability of the nanofiber matrix increased with the inclusion of BSA in the structure, potentially leading to an increased degradation rate. It was observed that the PVA/CH/HA/BSA-15 nanofiber group had the fastest degradation rate. A study on PVA/BSA hybrid hydrogels by Bercea et al. shows that at high BSA content, swelling rates and mass loss increase during swelling and degradation tests [33].

### 3.6. BSA drug release and kinetic studies

In the present study, an in vitro, drug release test was carried out in order to investigate the release property of BSA from electrospun nanofibers fabricated. As the initial step, the UV spectra for BSA with different concentrations from the range of 4–10 μg/ml to obtain BSA absorption values, peaks belonging to BSA were seen around 204 nm, which belonged to the backbone absorption of BSA [34], and the linear

**Table 3**
Transport models according to the range of n value.

| | Korsmeyer-Peppas | | Zero-Order | | First-Order | | Higuchi | | Hixon-Crowell | |
|---|---|---|---|---|---|---|---|---|---|---|
| Nanofibers | $R^2$ | n | $R^2$ | $K_o$ | $R^2$ | $K_1$ | $R^2$ | $K_H$ | $R^2$ | $K_{HC}$ |
| PVA/CH/HA/BSA-5 | 0,9758 | 63,646 | 0,8149 | 1236 | 0,977 | −0,0211 | 0,9265 | 13,232 | 0,971 | 0,0593 |
| PVA/CH/HA/BSA-10 | 0,9391 | 52,226 | 0,7496 | 1147 | 0,864 | −0,0209 | 0,8171 | 10,394 | 0,927 | 0,0532 |
| PVA/CH/HA/BSA-15 | 0,976 | 49,146 | 0,6887 | 1259 | 0,904 | −0,0211 | 0,8901 | 12,534 | 0,9381 | 0,0572 |

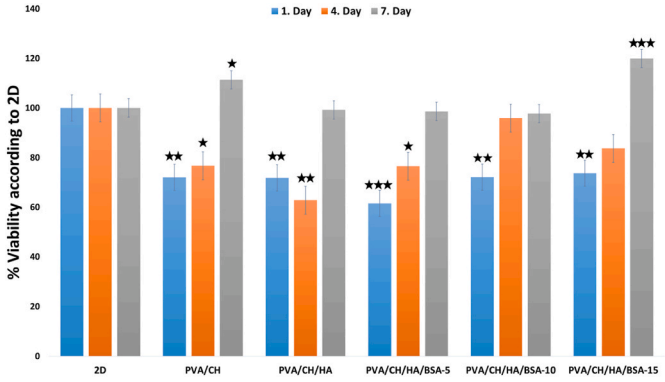


**Fig. 9.** Cell viability results of 1-day, 4-day, and 7-day treated materials. 2d culture was accepted as a control, and the calculations were compared with the control material. one-way analysis of variance, (ANOVA), Tukey-Kramer multiple comparisons test comparison to 2d, *p < 0,05, **p < 0,01, ***p < 0,001.

standard curve ($R^2 = 0.9827$) was plotted accordingly (Fig. 7(a & b)).

BSA release analyses were performed in PBS to increase the likeness of environmental conditions. In Fig. 7 (c), BSA release profiles of PVA/CH/HA/BSA-5, PVA/CH/HA/BSA-10, and PVA/CH/HA/BSA-15 was shown and each sample alone in Fig. 7 (c.1., c.2., and c.3.). For PVA/CH/HA/BSA-5 nanofiber, it can be seen that 58 % of BSA is released until 12th-hour ends, which exhibits a burst release profile. Similarly, PVA/CH/HA/BSA-10 and PVA/CH/HA/BSA-15 nanofibers also exhibit burst release profiles, %78 and %73 respectively within the 12th hour. All nanofibers continued to release BSA for the 72-h duration until %100 release occurred.

The release kinetic assessments of PVA/CH/HA/BSA-5, PVA/CH/HA/BSA-10, and PVA/CH/HA/BSA-15 nanofibers involved the application of various kinetic mathematical equations by Hixon-Crowell, Higuchi, Korsmeyer-Peppas, and Zero-Order, First-Order, as present in Fig. 8. Table 3., presents the kinetic constants and regression coefficients ($R^2$) obtained for all nanofibers during assessments with each mathematical model. For each nanofiber, the most appropriate mathematical description with the highest correlation coefficient was evaluated. The coefficients evaluated in Table 3 indicate that all nanofiber samples with BSA were governed by the first-order drug release model, as evidenced by the highest regression coefficient values among all models evaluated.

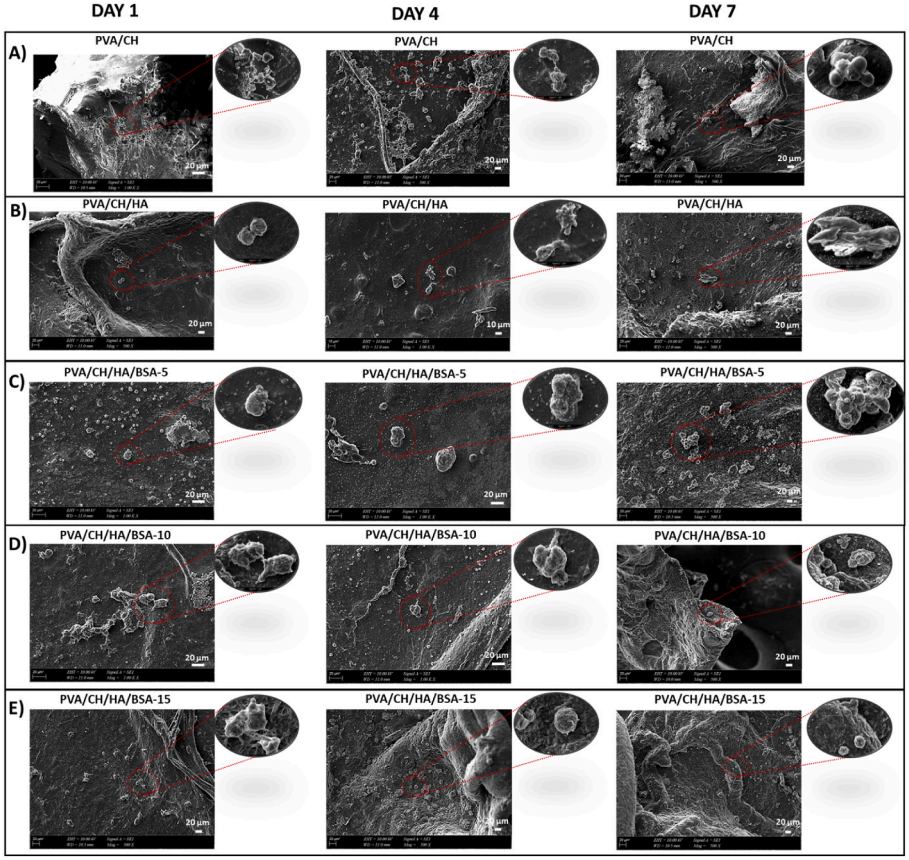


**Fig. 10.** SEM images of osteoblast cells cultured with PVA/CH (A), PVA/CH/HA (B), PVA/CH/HA/BSA-5 (C), PVA/CH/HA/BSA-10 (D), and PVA/CH/HA/BSA-15 (E) samples after 1, 3 and 7-days duration.

### 3.7. Biocompatibility and functional features of nanofibers

The biocompatibility of the nanofibers fabricated must be examined in order to understand the nanofiber's ability to not cause any toxic or disturbing effect on the host tissue [35]. The MTT assays were executed at 1, 4, and 7 days of incubation to understand and observe the effect of BSA on osteoblast cells (Cell line code: ATCC hFOB 1.19 CRL-3602 ™). Cell viability results of each fiber are shown in Fig. 9. According to the results, PVA/CH/HA/BSA-15 nanofiber exceeds the control group in terms of cell viability with 119.9 %. Among the rest of the BSA-containing samples, the second considerably successful nanofiber was PVA/CH/HA/BSA-10 nanofiber which reached 95.9 % on the 4th day and 97.7 on the 7th day. PVA/CH/BSA-5 nanofiber was able to reach 98.6 % cell viability at the completion of the 7th day. For the effect of BSA in terms of cell viability, results indicate a relation in a positive direction. Homaeigohar et al. [36], reports the PCL/BSA composite nanofibers and the influence of BSA on cell viability, mentions that due to the dissolution of BSA from the fiber, the nanofiber surface becomes rougher which provides a more stable surface for cells to attach with adhesion. Furthermore, the amine groups from BSA can cause positively charged nanofiber surfaces for negatively charged cells to attach with additional adhesion to nanofibers [36]. In agreement with the cell viability assay, SEM images from 1-day, 4-day, and 7-day cultured nanofiber samples in Fig. 10, showed increasing expansion, growth, and connection between cells on PVA/CH/HA/BSA nanofiber samples. Collected SEM images indicate that osteoblast cells were successfully attached to the nanofibers, and there were considerable growth and connectivity differences between samples without BSA and with.

## 4. Conclusion

In the present study, PVA/CH/HA/BSA with 0.05, 0.1, and 0.15 wt% BSA concentrations were fabricated via the electrospinning method successfully, for healing bone fractures/cracks and to contribute to bone tissue engineering applications. The SEM images indicate that nanofibers with BSA showed smooth surfaces and monodispersed fiber formation. Required porous structures were achieved, and the mean diameters of PVA/CH/HA/BSA-5, PVA/CH/HA/BSA-10, PVA/CH/HA/BSA-15 nanofibers were measured as 325.39 ± 77.512 nm, 332.45 ± 82.251 nm, 447.03 ± 101.382 nm respectively. However, degradation rates were controversial, on the 5th day almost 80 % of all the BSA-included nanofibers had degraded. In the case of BSA release, at the 12th hour burst release of BSA from all nanofibers was over, and controlled release of BSA continued till the 72nd hour. The MTT test outcomes indicated that biocompatible and non-cytotoxic nanofibers were fabricated. During 7 days of incubation with human osteoblast cells, the sample with PVA/CH/HA/BSA-15 exhibited the highest cell viability results, which could be possible due to the early release of BSA from nanofiber, which can cause a porous surface for new cells to attach, and initiate signaling among them to increase connectivity. Considering all the results from this study, PVA/CH/HA/BSA composite nanofibers can be a potential healing patch for bone fractures and cracks. In our future studies, we plan to use confocal microscope to study the cellular interaction of nanofibers.

## CRediT authorship contribution statement

**Mehmet Bozdag:** Writing – original draft, Methodology, Investigation. **Ferhat Urek:** Methodology, Investigation. **Sumeyye Cesur:** Writing – review & editing, Methodology, Conceptualization. **Ali Sahin:** Investigation, Conceptualization. **Oguzhan Gunduz:** Writing – review & editing.

## Declaration of competing interest

The authors declare that they have no known competing financial interests or personal relationships that could have appeared to influence the work reported in this paper.

## Acknowledgments

There is no funding support for this study.

## Data availability

The data that has been used is confidential.

## References

[1] A. Satpathy, A. Pal, S. Sengupta, A. Das, MdM. Hasan, I. Ratha, A. Barui, S. Bodhak, Bioactive nano-hydroxyapatite doped electrospun PVA-chitosan composite nanofibers for bone tissue engineering applications, J. Indian Inst. Sci. 99 (2019) 289–302, https://doi.org/10.1007/s41745-019-00118-8.
[2] R. Dimitriou, E. Jones, D. McGonagle, P. V Giannoudis, Bone regeneration: current concepts and future directions, BMC Med. 9 (2011) 66, https://doi.org/10.1186/1741-7015-9-66.
[3] U. Anjaneyulu, B. Priyadarshini, A. Nirmala Grace, U. Vijayalakshmi, Fabrication and characterization of Ag doped hydroxyapatite-polyvinyl alcohol composite nanofibers and its in vitro biological evaluations for bone tissue engineering applications, J. Sol. Gel Sci. Technol. 81 (2017) 750–761, https://doi.org/10.1007/s10971-016-4243-5.
[4] J.-H. Song, H.-E. Kim, H.-W. Kim, Electrospun fibrous web of collagen–apatite precipitated nanocomposite for bone regeneration, J. Mater. Sci. Mater. Med. 19 (2008) 2925–2932, https://doi.org/10.1007/s10856-008-3420-7.
[5] X. Lin, S. Patil, Y.-G. Gao, A. Qian, The bone extracellular matrix in bone formation and regeneration, Front. Pharmacol. 11 (2020), https://doi.org/10.3389/fphar.2020.00757.
[6] M.P. Lutolf, J.A. Hubbell, Synthetic biomaterials as instructive extracellular microenvironments for morphogenesis in tissue engineering, Nat. Biotechnol. 23 (2005) 47–55, https://doi.org/10.1038/nbt1055.
[7] D. Liang, B.S. Hsiao, B. Chu, Functional electrospun nanofibrous scaffolds for biomedical applications, Adv. Drug Deliv. Rev. 59 (2007) 1392–1412, https://doi.org/10.1016/j.addr.2007.04.021.
[8] S.R. Gavinho, M. Bozdag, C. Kalkandelen, J.S. Regadas, S.K. Jakka, O. Gunduz, F. N. Oktar, M.P.F. Graça, An eco-friendly process to extract hydroxyapatite from sheep bones for regenerative medicine: structural, morphologic and electrical studies, J. Funct. Biomater. 14 (2023) 279, https://doi.org/10.3390/jfb14050279.
[9] Z. Bal, T. Kaito, F. Korkusuz, H. Yoshikawa, Bone regeneration with hydroxyapatite-based biomaterials, Emergent Mater 3 (2020) 521–544, https://doi.org/10.1007/s42247-019-00063-3.
[10] I. Rajzer, E. Menaszek, R. Kwiatkowski, W. Chrzanowski, Bioactive nanocomposite PLDL/nano-hydroxyapatite electrospun membranes for bone tissue engineering, J. Mater. Sci. Mater. Med. 25 (2014) 1239–1247, https://doi.org/10.1007/s10856-014-5149-9.
[11] S. Cesur, E. Ilhan, E. Pilavci, R.B. Sulutas, M. Gurboga, O. Bingol Ozakpinar, E. Kaya, M. Heljak, G. Bosgelmez Tinaz, F.N. Oktar, O. Gunduz, E. Kijeńska-Gawrońska, A novel strategy as a potential rapid therapy modality in the treatment of corneal ulcers: fluconazole/vancomycin dual drug-loaded nanofibrous patches, Macromol. Mater. Eng. 308 (2023), https://doi.org/10.1002/mame.202200697.
[12] A.Sh Asran, S. Henning, G.H. Michler, Polyvinyl alcohol–collagen–hydroxyapatite biocomposite nanofibrous scaffold: mimicking the key features of natural bone at the nanoscale level, Polymer (Guildf) 51 (2010) 868–876, https://doi.org/10.1016/j.polymer.2009.12.046.
[13] G.-M. Kim, P. Simon, J.-S. Kim, Electrospun PVA/HAp nanocomposite nanofibers: biomimetics of mineralized hard tissues at a lower level of complexity, Bioinspir Biomim 3 (2008) 046003, https://doi.org/10.1088/1748-3182/3/4/046003.
[14] C.P. Jiménez-Gómez, J.A. Cecilia, Chitosan: a natural biopolymer with a wide and varied range of applications, Molecules 25 (2020) 3981, https://doi.org/10.3390/molecules25173981.
[15] I. Shirzaei Sani, M. Rezaei, A. Baradar Khoshfetrat, D. Razzaghi, Preparation and characterization of polycaprolactone/chitosan-g-polycaprolactone/hydroxyapatite electrospun nanocomposite scaffolds for bone tissue engineering, Int. J. Biol. Macromol. 182 (2021) 1638–1649, https://doi.org/10.1016/j.ijbiomac.2021.05.163.
[16] C.M. Valmikinathan, S. Defroda, X. Yu, Polycaprolactone and bovine serum albumin based nanofibers for controlled release of nerve growth factor, Biomacromolecules 10 (2009) 1084–1089, https://doi.org/10.1021/bm8012499.
[17] C. Tang, A.E. Ozcam, B. Stout, S.A. Khan, Effect of pH on protein distribution in electrospun PVA/BSA composite nanofibers, Biomacromolecules 13 (2012) 1269–1278, https://doi.org/10.1021/bm2017146.
[18] F. Roozbahani, N. Sultana, D. Almasi, F. Naghizadeh, Effects of Chitosan Concentration on the Protein Release Behaviour of Electrospun Poly(ε-caprolactone)/Chitosan Nanofibers, J. Nanomater. (2015) 1–11, https://doi.org/10.1155/2015/747420, 2015.
[19] E. Ilhan, Z. Karahaliloglu, E. Kilicay, B. Hazer, E.B. Denkbas, Potent bioactive bone cements impregnated with polystyrene-g-soybean oil-AgNPs for advanced bone tissue applications, Mater. Technol. 35 (2020) 179–194, https://doi.org/10.1080/10667857.2019.1661157.

[20] E. Ilhan, S. Ulag, A. Sahin, N. Ekren, O. Kilic, F.N. Oktar, O. Gunduz, Production of 3D-printed tympanic membrane scaffolds as a tissue engineering application. https://doi.org/10.1007/978-3-030-45385-5_16, 2020.
[21] E. Ilhan, S. Cesur, R.B. Sulutas, E. Pilavci, B. Dalbayrak, E. Kaya, E.D. Arisan, G. B. Tinaz, M. Sengor, E. Kijeńska-Gawrońska, F.N. Oktar, O. Gunduz, The role of multilayer electrospun poly(vinyl alcohol)/gelatin nanofibers loaded with fluconazole and cinnamaldehyde in the potential treatment of fungal keratitis, Eur. Polym. J. 176 (2022) 111390, https://doi.org/10.1016/j.eurpolymj.2022.111390.
[22] S.A. Salim, S.A. Loutfy, E.M. El-Fakharany, T.H. Taha, Y. Hussien, E.A. Kamoun, Influence of chitosan and hydroxyapatite incorporation on properties of electrospun PVA/HA nanofibrous mats for bone tissue regeneration: nanofibers optimization and in-vitro assessment, J. Drug Deliv. Sci. Technol. 62 (2021) 102417, https://doi.org/10.1016/j.jddst.2021.102417.
[23] R. Fazel, S.-F. Torabi, P. Naseri-Nosar, S. Ghasempur, S.-O. Ranaei-Siadat, K. Khajeh, Electrospun polyvinyl alcohol/bovine serum albumin biocomposite membranes for horseradish peroxidase immobilization, Enzym. Microb. Technol. 93–94 (2016) 1–10, https://doi.org/10.1016/j.enzmictec.2016.07.002.
[24] C. Zhang, X. Yuan, L. Wu, Y. Han, J. Sheng, Study on morphology of electrospun poly(vinyl alcohol) mats, Eur. Polym. J. 41 (2005) 423–432, https://doi.org/10.1016/j.eurpolymj.2004.10.027.
[25] G.C. da Mata, M.S. Morais, W.P. de Oliveira, M.L. Aguiar, Composition effects on the morphology of PVA/chitosan electrospun nanofibers, Polymers 14 (2022) 4856, https://doi.org/10.3390/polym14224856.
[26] C. Risdian, M. Nasir, A. Rahma, H. Rachmawati, The influence of formula and process on physical properties and the release profile of PVA/BSA nanofibers formed by electrospinning technique, J. Nano Res. 31 (2015) 103–116. https://dx.doi.org/10.4028/www.scientific.net/JNanoR.31.103.
[27] T. Siddaiah, P. Ojha, N.O.G.V.R. Kumar, C. Ramu, Structural, optical and thermal characterizations of PVA/MAA:EA polyblend films, Mater. Res. 21 (2018), https://doi.org/10.1590/1980-5373-mr-2017-0987.
[28] M. Koosha, H. Mirzadeh, Electrospinning, mechanical properties, and cell behavior study of chitosan/<scp>PVA</scp> nanofibers, J. Biomed. Mater. Res. 103 (2015) 3081–3093, https://doi.org/10.1002/jbm.a.35443.
[29] T. Li, X. Ding, L. Tian, S. Ramakrishna, Engineering BSA-dextran particles encapsulated bead-on-string nanofiber scaffold for tissue engineering applications, J. Mater. Sci. 52 (2017) 10661–10672, https://doi.org/10.1007/s10853-017-1245-9.
[30] M. Bercea, L.-M. Gradinaru, S. Morariu, I.-A. Plugariu, R.V. Gradinaru, Tailoring the properties of PVA/HPC/BSA hydrogels for wound dressing applications, React. Funct. Polym. 170 (2022) 105094, https://doi.org/10.1016/j.reactfunctpolym.2021.105094.
[31] A. Çay, M. Miraftab, E. Perrin Akçakoca Kumbasar, Characterization and swelling performance of physically stabilized electrospun poly(vinyl alcohol)/chitosan nanofibres, Eur. Polym. J. 61 (2014) 253–262, https://doi.org/10.1016/j.eurpolymj.2014.10.017.
[32] P. Ma, W. Wu, Y. Wei, L. Ren, S. Lin, J. Wu, Biomimetic gelatin/chitosan/polyvinyl alcohol/nano-hydroxyapatite scaffolds for bone tissue engineering, Mater. Des. 207 (2021) 109865, https://doi.org/10.1016/j.matdes.2021.109865.
[33] M. Bercea, I.-A. Plugariu, M.V. Dinu, I.M. Pelin, A. Lupu, A. Bele, V.R. Gradinaru, Poly(Vinyl alcohol)/bovine serum albumin hybrid hydrogels with tunable mechanical properties, Polymers 15 (2023) 4611, https://doi.org/10.3390/polym15234611.
[34] E. Bronze-Uhle, B.C. Costa, V.F. Ximenes, P.N. Lisboa-Filho, Synthetic nanoparticles of bovine serum albumin with entrapped salicylic acid, Nanotechnol. Sci. Appl. 10 (2016) 11–21, https://doi.org/10.2147/NSA.S117018.
[35] S. Harmanci, A. Dutta, S. Cesur, A. Sahin, O. Gunduz, D.M. Kalaskar, C. B. Ustundag, Production of 3D printed Bi-layer and tri-layer sandwich scaffolds with polycaprolactone and poly (vinyl alcohol)-metformin towards diabetic wound healing, Polymers 14 (2022) 5306, https://doi.org/10.3390/polym14235306.
[36] S. Homaeigohar, M. Monavari, B. Koenen, A.R. Boccaccini, Biomimetic biohybrid nanofibers containing bovine serum albumin as a bioactive moiety for wound dressing, Mater. Sci. Eng. C 123 (2021) 111965, https://doi.org/10.1016/j.msec.2021.111965.